Fatigue Properties of Electron Beam Welded Precipitation Hardening Stainless Steels

The fatigue properties of several electron beam welded precipitation hardening stainless steels are compared with unwelded specimens

BY A. A. WARE AND E. R. FUNK

ABSTRACT. The fatigue properties of unwelded and electron beam welded PH 14-8 Mo, Ph 14-8 Mo Vac Melt, and Ph 15-7 Mo precipitation hardening stainless steels have been investigated. Fatigue tests were conducted on specially designed plate specimens in a Krouse fatigue testing machine using complete stress reversal. Specimens were then tested in the heat-treated condition. Micro hardness traverses were taken across typical fusion zones after welding and are reported. Finally, fatigue curves for these materials in the welded and unwelded conditions are presented.

The electron beam welded specimens showed significantly decreased fatigue properties. This result was attributed to the very narrow but still significant heat affected zone.

The fatigue properties determined for PH 14-8 Mo, PH 14-8 Mo Vac Melt, and PH 15-7 Mo precipitation hardening stainless steels indicated that no endurance limit was reached within the maximum test range of 1.5×10^6 cycles.

The fatigue properties of unwelded specimens were rated in terms of fatigue ratio at 1.5×10^6 cycles. Maximum fatigue performance was recorded by PH 14-8 Mo Vac Melt stainless steel, with PH 14-8 Mo and PH 15-7 Mo stainless steels following in a decreasing order of fatigue performance.

A comparison between materials produced by vacuum melting and arc-furnace melting processes indicated that the vaccum melting process accounted for a 20 to 30% increase in the fatigue life of PH 14-8 Mo stainless steels.

Electron beam welded fatigue joint efficiencies of 40 to 75 were recorded for the PH 14-8 Mo Vac Melt, while efficiencies of 30 to 54% were recorded for the PH 14-8 Mo specimens.

Introduction

In 1959 electron beam welding emerged from the laboratory, no longer a curosity but a production tool. This unique process was characterized by three main advantages over more conventional welding processes:[1]

1. It permitted a weldment to be fabricated with a low total energy input into the workpiece.
2. The low energy input enabled very accurate control of the intensity and position of the beam.
3. The process was carried out in a vacuum which eliminated contamination of the workpiece. (Since a vacuum of the order of 1/10,000,000th atmospheric pressure is required for the electron beam to operate, weld fusion zones are relatively free of absorbed gases.)

Presently the electron beam welding process is being considered for more practical applications. These applications are especially numerous in the aerospace and nuclear industries.

The electron beam process, with its extremely high energy density beam, has adapted itself well to industrial needs especially since the deep penetrating beam imparts a minimum of distortion to the piece(s) being welded as well as yielding a fusion zone which is as frec of contamination as the base metal.

Process Characteristics

Weld Bead Shape and Heat-Affected Zone Size

Perhaps the most unique feature of electron beam weldments is the ratio of penetration to width in the weld bead which may approach 25 to 1. Extensive research carried out to Hashimoto and Matsuda[2, 3] has resulted in an explanation for the unique bead shape and ratio of penetration to width in an electron beam weldment.

Obviously, if less heat enters the welded material and if the heat which enters the plate can be dissipated along the entire depth of penetration, then the resulting heat-affected zone will be minimized. The magnitude of this consequence is shown in Fig. 1 in work done by Meier.[1]

In many applications, weldments undergo numerous loading cycles which decrease the magnitude of the safe stress level that the weldments can endure without failure. Therefore, if the electron beam welding process is to receive full consideration as in industrial joining process, a more complete knowledge of the fatigue properties of the electron beam weldments must be made available to designers.

In accordance with the needs of advancing the state of the art, a fatigue study program was undertaken. Three relatively new precipitation hardening stainless steels of the high strength variety were investigated. Since the materials were recently developed, fatigue data were not available for these materials in the unwelded condition. Consequently, both unwelded and electron beam welded specimens were tested in order to compile a comparitive description of the fatigue properties of the materials.

Fatigue Hardening and Metallurgical Benefits of Electron Beam Welding

The benefits to be expected from electron beam welding in improving the fatigue performance of a weldment by eliminating weld defects are numerous. In electron beam welding, incomplete penetration, porosity, and inclusions may be controlled to the point that these defects no longer are the initiators of fatigue failure. Unfortunately, the great wealth of empirical data on fatigue failure does not make up for the lack of knowledge concerning the fatigue failure mechanism. Specific knowledge of this failure mechanism is needed in order to relate fatigue failure to the metal-

A. A. WARE is Research Assistant and E. R. FUNK is Associate Professor, Department of Welding Engineering, The Ohio State University, Columbus, Ohio.

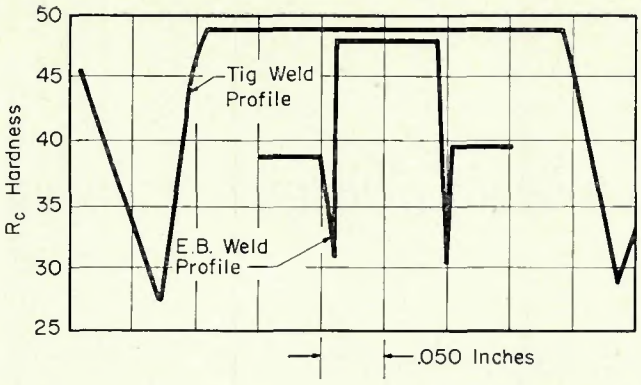

Fig. 1—Hardness profile comparing an electron beam weld and a gas tungsten-arc weld in AISI 4340; note the relative sizes of the soft temper zones[1]

lurgical properties of the weld material, particularly the microstructure of the heat-affected and fusion zones.

Due to the vacuum remelt quality of the fusion zone and due to the extremely short thermal cycle which produces relatively small heat-affected zones with minimum grain coarsening and precipitate redistribution, electron beam welding has been considered for applications where optimum fatigue properties are required in welded joints. Hopefully, weldments which match the fatigue properties of the non-welded base materials will be produced.

Previous Investigations

Initial electron beam fatigue information was published by Meier[1] on tests conducted using AISI 4340 weldments.—Fig. 1.

In more recent work Roth, Bratkovich, and Purdy[4] determined the fatigue performance of high strength alloy weldments for aircraft turbine engine gears. In general, electron beam weldments exhibited joint efficiencies 85% of the parent metal endurance limits.

Hofmann, Koch, and Sceler[5] have investigated the mechanical properties of $^{18}/_{8}$ austenitic Cr/Ni which were electron beam welded. Two alloy compositions were analyzed in this study, columbium (I) stabilized material, and titanium (II) stabilized material. Fatigue tests revealed the weldments were 13% weaker in endurance limits than the base material. Since all observed cracks originated in the heat-affected zone of the weldments, it was suggested that this zone produced a notch affect in the material thus initiating failure.

McHenry, Collins, and Key[6, 7] have compiled a comprehensive electron beam weldment fatigue study on $^{1}/_{2}$ in. thick D6AC high strength steel (220–240 and 260–280 ksi tensile strengths). Initial tests indicated that the fatigue performance of electron beam weldments would be inadequate for the desired application. Metallographic and fractographic examinations revealed that interdendritic cracks oriented parallel to the loading direction acted as initiation sites for fatigue cracks, but did not affect the tensile properties of the weldment.

Rapid solidification inward, induced by the concentrated heat input characteristic of all electron beam welds, generated interdendritic voids upon cooling. These voids were the crack initiation sites. McHenry *et al* [6] hypothesized that if the solidification pattern was altered by oscillation of the beam, the interdendritic voids would be eliminated. Further tests indicated that beam oscillation did change the solidification pattern, and thus broaden the weld zone.

A new series of fatigue tests were then conducted. In all cases the fatigue performance of the electron beam weldment was superior to previous work. Failures still originated in the weld zone, but pin hole porosity served as stress concentration sites for initiating fatigue failure.

Experimental Procedure

Materials

Two types of precipitation hardening stainless steels were employed in this investigation. These materials designated PH 14-8 Mo and PH 15-7 Mo by the Armco Steel Corporation are essentially high strength chromium-nickel steels that exhibit exceptional corrosion resistance in the heat treated condition. Due to the precipitation hardening capability of these alloy steels, it is possible to fabricate the materials in the soft austenitic condition and subsequently perform the necessary heat treatment in order to obtain the high strength-high fracture toughness mechanical properties.

All test materials were received in the condition indicated in Table 1. Ladle analysis compositions of each material were provided along with the

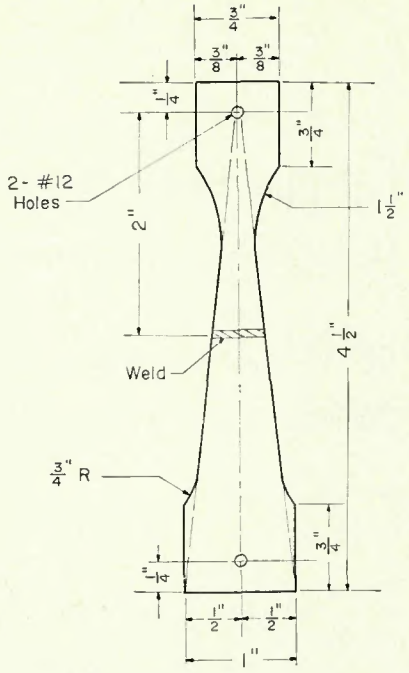

Fig. 2—Fatigue test specimen machined from $^{1}/_{8}$ in. plate, all dimensions have a $\pm$ $^{1}/_{64}$ in. tolerance. Direction of rolling from top to bottom

heat designations. It should be noted that two types of PH 14-8 Mo material were provided. One was a vacuum melted product while the other was an ordinary arc-furnace product. Henceforth, for the purposes of this paper, the materials will be referred to as PH 14-8 Mo Vac Melt and PH 14-8 Mo. In the initial communications with Armco Steel it was ascertained that, although all materials, (as-received) were $^{1}/_{8}$ in. thick sheet stock, the PH 14-8 Mo Vac Melt had to be rolled in the laboratory in order to meet the desired dimensions. This accounted for the slightly higher hardnesses recorded for the vacuum melted material in the as-welded condition.

General Procedure and Apparatus

A fatigue specimen was designed that could be accommodated in the Krouse fatigue testing machine. This type of fatigue machine relies on cyclic flexure to produce cyclic loading by bending the plate specimens.

The specially designed specimen employed in this test is shown in Fig. 2. The stress level for any particular load is constant over the entire linearly tapered length of the specimen. Therefore, the weldment could conceiveably be placed anywhere in this section and be stressed identical to the base material. Previous experience with the general design made it advisable to place the weld across the mid-point of the specimen. This facilitated the preparation of weld test plates because they could be cut to the

same size.

The butting surfaces of the welded test plates were subsequently ground, wire brush finished, and cleaned in acetone prior to welding.

Welding

A Hamilton-Zeiss Model W1-0 electron beam welding machine was employed to weld the stainless steel. This welding machine had a 4.5 kw capacity, with a maximum attainable beam current of 30 ma and a maximum accelerating potential of 150 kv. Beam focus controls enabled beam spots of 0.010 in. in diameter to be achieved, while table speed was regulated from 5 to 120 ipm.

Welded plates were fitted in a small fixture that was fabricated in order to maintain joint alignment once the electron beam had been energized.

It was decided to employ a cap strip of identical composition to the base metal on top of the joint, in order to provide the necessary filler metal. This procedure assured that the weld metal composition would be identical to the base metal and also alleviated the undercut problem since the cap strip along with the bottom reinforcement could be machined off after welding. This procedure necessitated making a full penetration weld in $^1/_4$ in. of the stainless steel which approached the power capacity of the equipment. Table 2 lists the final welding parameters that were found acceptable.

Fatigue specimens were machined from welded and unwelded test plates according to the specifications in Fig. 2. Special care was taken to note that the direction of rolling be identical in all specimens. Such a variation in specimens could greatly increase the scatter in fatigue performance.

After machining all specimens were measured in order to assure dimensional accuracy. Identification numbers were given to each specimen for future reference.

A series of grinding and polishing operations was the next step in preparing the specimens for fatigue testing.

Heat Treatment

After welding and final polishing, the specimens were precipitation heat treated by austeniting at 1750° F in an argon atmosphere. Complete martensite transformation was accomplished by cooling to 100° F and holding for 8 hr. Final strengthening of the martensite matrix was achieved by a precipitation hardening reaction carried out at 1050 or 950° F (depending upon the alloy) and holding this temperature for 1 hr. Heat treatment specification as described by Armco Steel[8] are given in Table 3.

The final precipitation treatment resulted in slight specimen discoloration which was removed by polishing with 400 grit in the rolling direction.

All-welded specimens were nondestructively tested by liquid penetrant and radiography to determine their pretest condition. Indications of

Table 1—Test Material Data

Materials used:

Steel type and heat	Ladle analyses, % C	Mn	P	S	Si	Cr	Ni	Mo	Al
PH 15-7 Mo (860569)	.067	.74	.011	.017	.43	15.18	7.00	2.24	1.22
PH 14-8 Mo (31562)	.040	.28	.008	.003	.67	14.38	8.14	2.00	1.22
PH 14-8 Mo (V5403)	.031	.05	.004	.004	.05	15.27	8.45	2.25	1.12

Material condition:

Heat	Heat treatment		Melting process
860569	Mill anneal	Condition A	Arc-furnace
31562	Mill anneal	Condition A	Arc-furnace
V5403	Mill anneal	Condition A	Vacuum melted

Mechanical properties:

Property	PH 14-8 Mo (Vac Melt and arc-furnace)[a]	PH 15-7 Mo (Arc-furnace)[b]
Ultimate tensile strength, ksi	200	240
0.2% yield strength, ksi	180	225
Elongation in 2 in. ,%	4	6
Hardness, R_c	38/45	46/48

[a] Condition SRH 1050.
[b] Condition RH 950.

Table 2—Welding Parameters

Welding parameters	Plate identification[a] 1A	1B	1C	2A	2B	2C	3A	3B	3C
Beam current, ma	15.0	15.0	15.0	12.5	12.8	13.0	15.1	15.1	15.1
Accelerating potential, kv	130	130	130	130	130	130	130	130	130
Filament current, amp	.80	.80	.80	.76	.76	.76	.80	.80	.80
Focus current, amp	.56	.55	.55	.61	.62	.57	.54	.54	.54
Travel speed, ipm	22.5	22.5	22.5	22.5	22.5	22.5	22.5	22.5	22.5
Focus note	Slight beam defocus employed on all welds								
Vacuum	Varied between 2.5×10^{-4} mm Hg to 1.0×10^{-4} mm Hg								

[a] Note plate series: 1A, 1B, 1C—PH 14-8 Mo arc melt; 2A, 2B, 2C—PH 15-7 Mo arc melt; 3A, 3B, 3C—PH 14-8 Mo vacuum melt.

Table 3—Material Heat Treatment Flow Chart

PH 14-8 Mo Arc-furnace and Vac Melt	PH 15-7 Mo Arc-furnace melt
I. Annealed 1825 ± 25° F at mill *Condition A*	I. Annealed 1950 ± 25° F at mill *Condition A*
II. Fabricate	II. Fabricate
III. Austenite conditioning Heat to 1700 ± 15° F Hold for 60 min Air cool to 75° F *Condition A1700*	III. Austenite conditioning Heat to 1750 ± 15° F Hold for 10 min. Air cool to R. T. *Condition A175C*
IV. Transformation Within 60 min. Cool to −100 ± 10° F Hold for 8 hrs. *Condition SR100*	IV. Transformation Within 60 min. Cool to −100 ± 10° F Hold for 8 hrs. *Condition R100*
V. Precipitation Hardening Heat to 1050 F ± 10° F Cool to R.T. *Condition SRY1050*	V. Precipitation Hardening Heat to 950 F ± 10° F Cool to R.T. *Condition RY950*

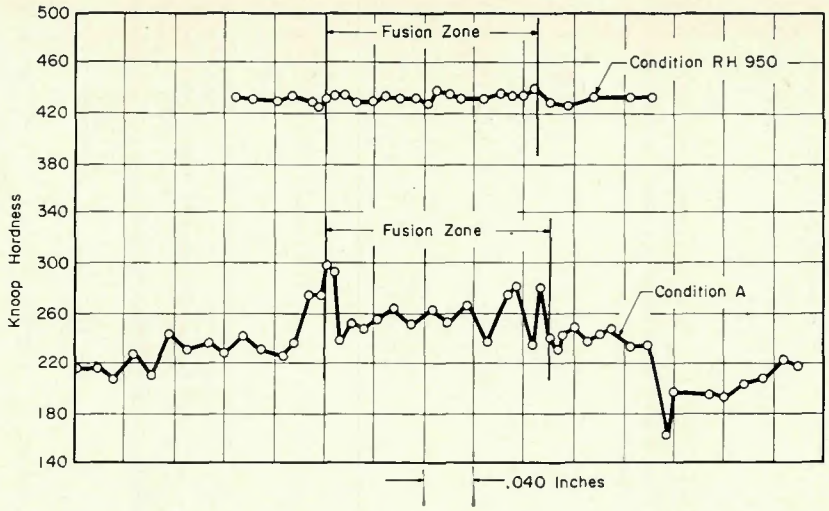

Fig. 3—Microhardness traverses of PH 15-7 Mo stainless steel electron be m welded; hardness surveys taken before heat treatment in *Condition A* and af e heat treatment in *Condition RY 950*

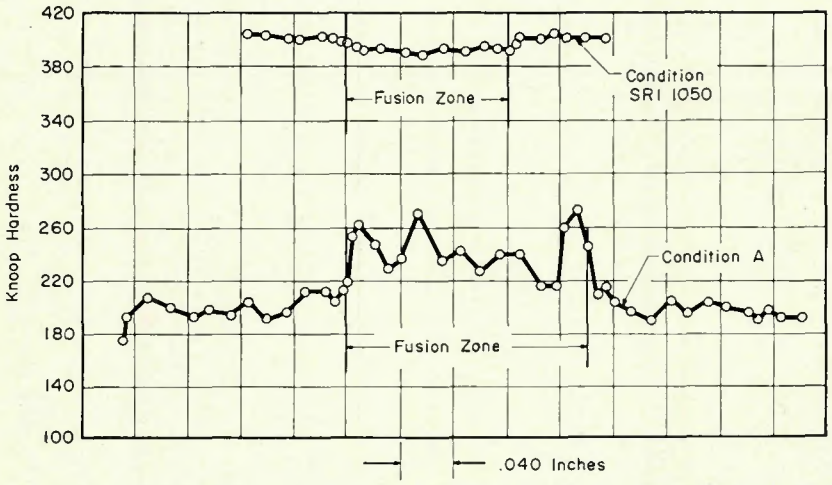

Fig. 4—Microhardness traverses of PH 14-8 Mo stainless steel electron beam welded; hardness surveys taken before heat treatment in *Condition A* and after heat treatment in *Condition SRH 1050*

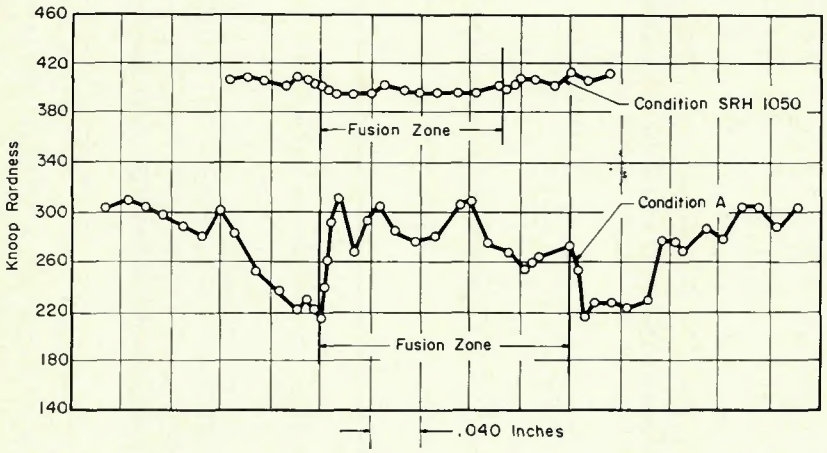

Fig. 5—Microhardness traverses of PH 14-8 Mo vacuum melt stainless steel electron beam welded; hardness surveys taken before heat treatment in *Condition A* and after heat treatment in *Condition SRH 1050*

pretest defects eliminated specimens from the fatigue test procedure.

In order to increase the confidence of the results, 5 specimens were tested at each load level in the unwelded condition and 3 specimens for the welded condition. Due to variations in the dimensions, the resulting stresses did vary to some degree. For the welded specimens, the experience gained from testing the unwelded specimens enabled a more judicious choice of stress levels to be made.

Fatigue curves were then determined by averaging the stresses at each load value and by determining the normal distribution of cycles to failure (or 1.5×10^6) cycles at the stress level under consideration.

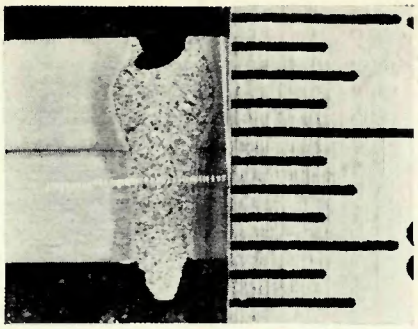

Fig. 6—Photomacrograph of PH 15-7 Mo electron beam weldment. Top strip is the filler metal cap strip. Hardness traverse is in specimen material. Scale on right is in $^1/_{32}$ in. divisions

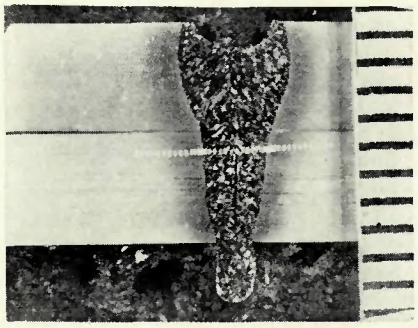

Fig. 7—Photomacrograph of PH 14-8 Mo electron beam weldment. Top strip is the filler metal cap strip. Hardness traverse is in specimen material. Scale on right is in $^1/_{32}$ in. divisions

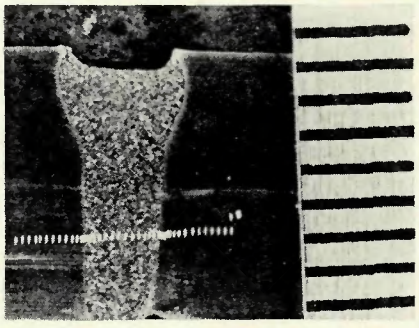

Fig. 8—Photomacrograph of PH 14-8 Mo Vac Melt electron beam weldment. Top strip is the filler metal. Scale on right is in $^1/_{32}$ in. divisions

Experimental Results

Microhardness Surveys

Microhardness traverses were taken across typical fusion zones after weld-

ing to determine the affects of the electron beam heat input upon the base metal. The lower curves in Figs. 3–5 show these surveys. PH 15-7 Mo and PH 14-8 Mo exhibited heat-affected zones approximately 0.040 in. wide. These zones are too small to be seen in microscopic observations (Figs. 15 and 16). As seen in Figs. 6 and 7, the surveys were taken in the lower strip of material, which would be the fatigue specimen. The upper strip of metal was the cap strip used as the filler metal and later machined off. The heat-affected zone in these two materials showed a definite increase in hardness of approximately 80 Knoop units.

Previously it was stated that the PH 14-8 Mo Vac Melt had been cold rolled in the laboratory before delivery. Consequently, the base material as seen in Fig. 5 is definitely harder than the PH 14-8 Mo base metal. The heat-affected zone in this weldment (PH 14-8 Mo Vac Melt) was about 0.80 in. wide and exhibited a decrease in hardness of approximately 80 Knoop units. Quite evidently this was a consequence of heating the cold rolled material in a highly localized region. The photomacrograph in Fig. 8 shows the fusion zone and heat-affected zone for the vacuum melted material.

After the heat-treatment cycles were concluded, another series of microhardness traverses were taken. Two specific purposes were intended for the second survey:

1. To check the accuracy of the heat treatment cycle.
2. To determine the resulting sizes of the heat affected zones.

The upper curve in Figs. 3–5 indicates that in the heat-treated condition no heat-affected zones were in existence. The fusion zone was approximately 5 to 10 Knoop units softer than the unwelded base metal in both PH 14-8 Mo alloy steels.

Macroscopic Examination of Fusion Zone

The fusion zones of all weldments were polished and etched using standard metallographic techniques. An electrolytic bath was used with an oxalic acid solution at 400 ma for 20 to 30 sec in order to etch specimens.

Fusion zones of all weldments exhibited distinct dendrites oriented perpendicular to the line of direction of the electron beam. Figure 7 shows this structure clearly. The distinct weld centerline is very evident in this picture. Postheat treatment macroscopic examinations did not reveal any significant change in the fusion zone structure, although dentrites seemed to be slightly narrower than in the as-welded condition.

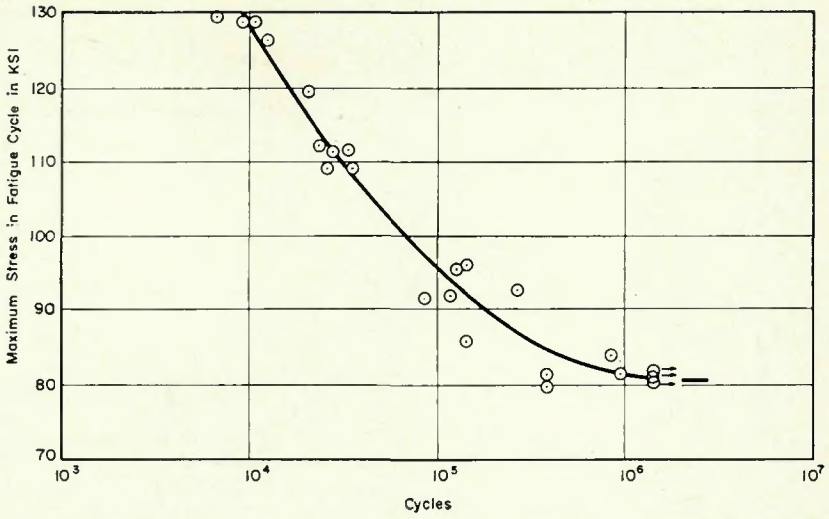

Fig. 9—Fatigue life of PH 14-8 Mo Vac Melt stainless steel in heat-treated *Condition SRH 1050*

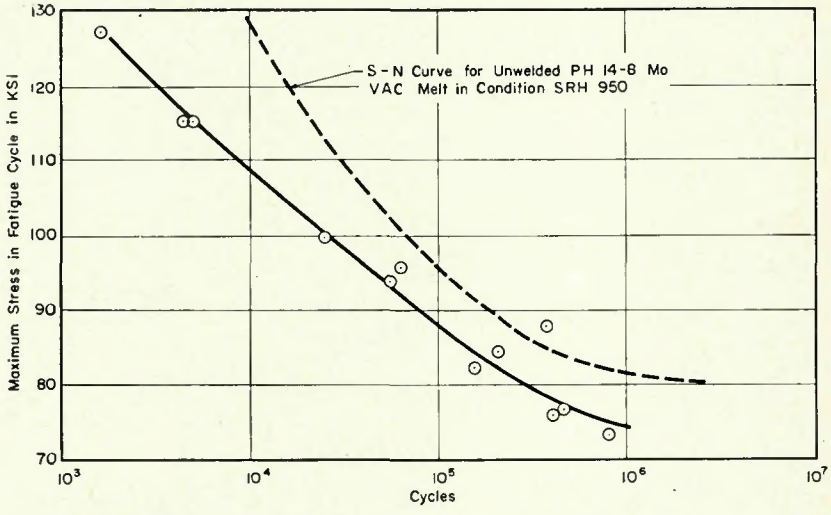

Fig. 10—Fatigue life of PH 14-8 Mo Vac Melt stainless steel electron beam welded and subsequently heat treated to *Condition SRH 1050*

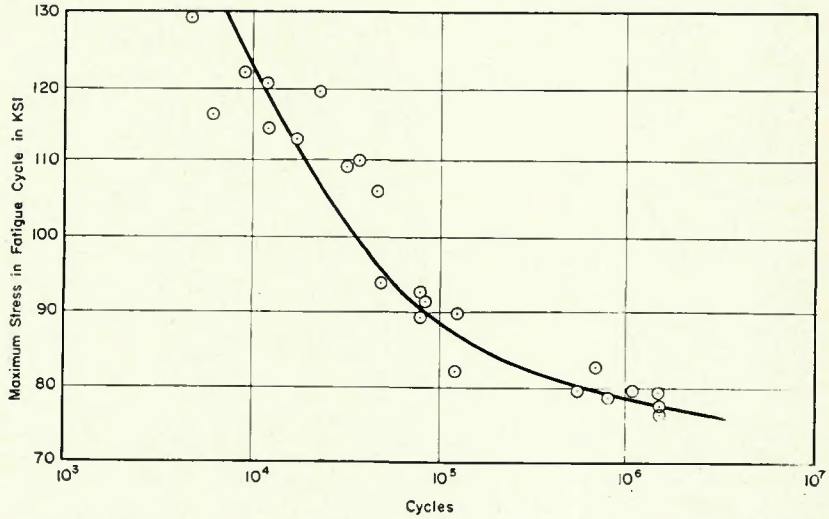

Fig. 11—Fatigue life of PH 14-8 Mo stainless steel in heat treated *Condition SRH 1050*

Unwelded Fatigue Specimen Tests

Fatigue curves for the 3 materials

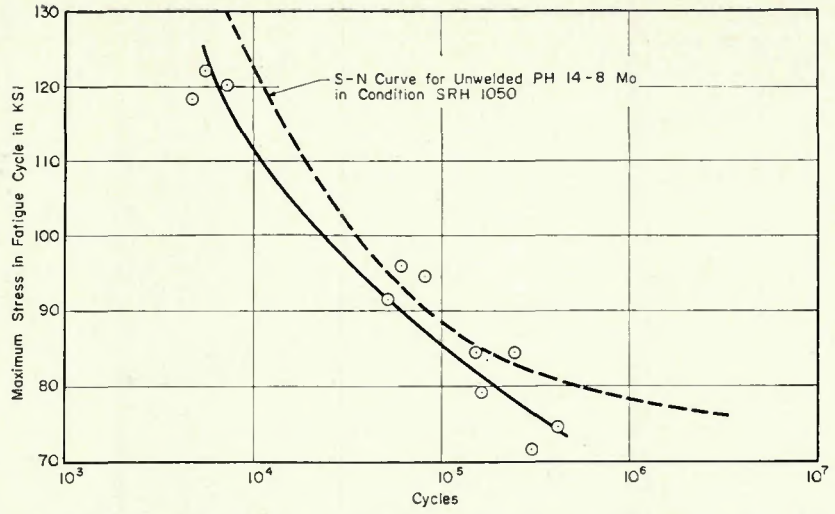

Fig. 12—Fatigue life of PH 14-8 Mo stainless steel electron beam welded and subsequently heat treated to *Condition SRH 1050*

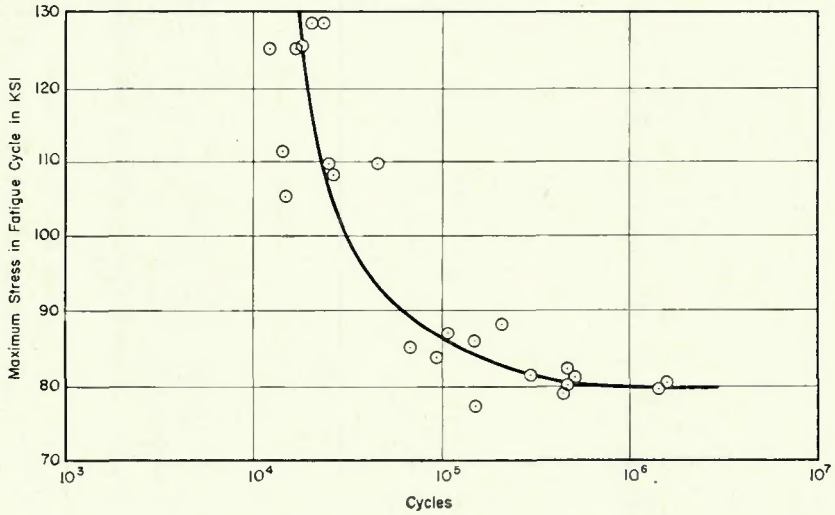

Fig. 13—Fatique life of PH 15-7 Mo stainless steel in heat-treated *Condition RH 950*

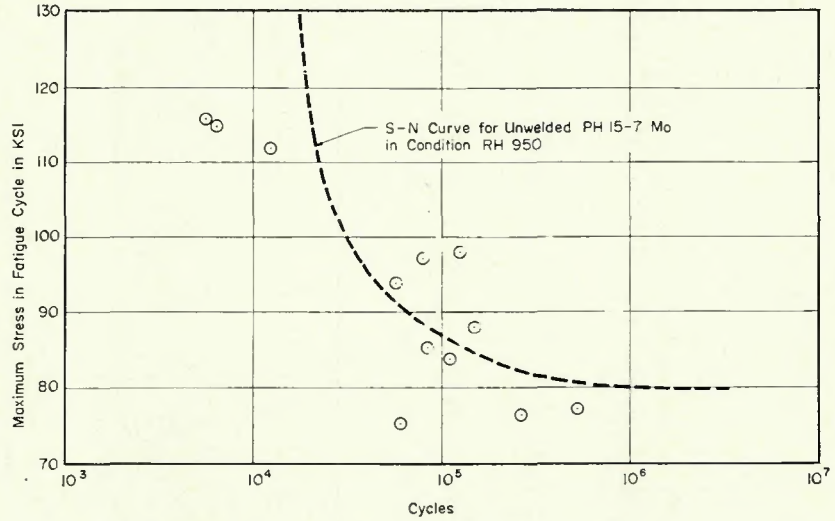

Fig. 14—Fatigue life of PH 15-7 Mo stainless steel electron beam welded and subsequently heat treated to *Condition RH 950*

under investigation are drawn in Figs. 9–11.

Comparing the fatigue curves for the arc-furnace and vacuum melted PH 14-8 Mo materials indicated that the fatigue life of the vacuum melted material was 20 to 30% superior to the arc-furnace material at all stress levels. The endurance limit of the vacuum melted material approached 81,000 psi, while that of the arc-furnace melt approached 77,000 psi. Although the fatigue properties of the PH 15-7 Mo at low cycle life were superior to the PH 14-8 Mo heats, the overall performance was inferior below 115,000 psi. The endurance limit of the PH 15-7 Mo was 80,000 psi, or less than the vacuum melted PH 14-8 Mo, although the tensile strength of the former was 45,000 psi higher than the latter.

Fatigue failure occurred in the tapered section of the specimen arm in 72% of the unwelded fatigue fractures. Only 14.5% of the fractures were initiated in the clamp vise. Failures in the tapered section of unwelded specimens were recorded between 1½ to 2¼ in. from the base end of the specimen.

Welded Fatigue Specimen Tests

Fatigue curves for electron beam welded specimens are given in Figure 12–14. S-N curves were plotted using the same procedure as employed for the unwelded specimens. The broken line in each figure represents the S-N curve for the unwelded specimens heat treated to the same condition as the welded specimens.

Approximately 92% of the fatigue failures that were recorded in welded specimens were initiated and propagated in the fusion zones. While fatigue tests were in progress, the propagation of the fatigue crack(s) along the surface of the specimens could be observed. In every observable case the crack was seen to propagate within the boundaries of the fusion zone adjacent to the fusion line. In a number of specimens, fatigue cracks propagated from opposite sides of the specimen, on opposite sides of the fusion zone. When the two cracks propagated to the center of the specimen, the two cracks crossed the weld center line to complete the fracture. Both examples are illustrated in Fig. 15. Fatigue fractures are shown in Fig. 16.

Fatigue joint efficiencies were calculated for the electron beam welded specimens. Joint efficiencies of 40 to 74% were calculated for the PH 14-8 Mo weldments. Thirty to 54% joint efficiencies were recorded for the PH 14-8 Mo Vac Melt weldments. No calculations were available for the PH 15-7 Mo because of the extremely large amount of scatter that was encountered in the data. Comparing the two heats of PH 14-8 Mo, it was observed that the fatigue performance of the vacuum melted material only

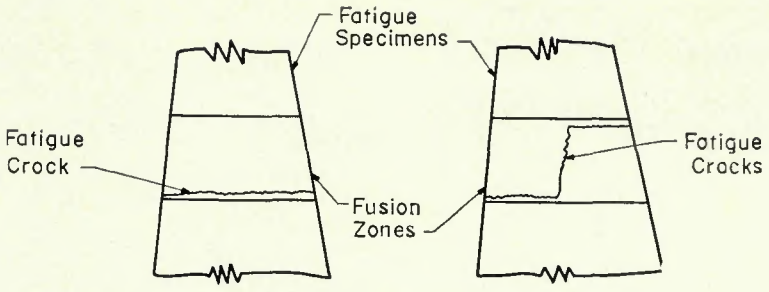

Fig. 15—Two fusion zone fatigue fractures typical to most specimens

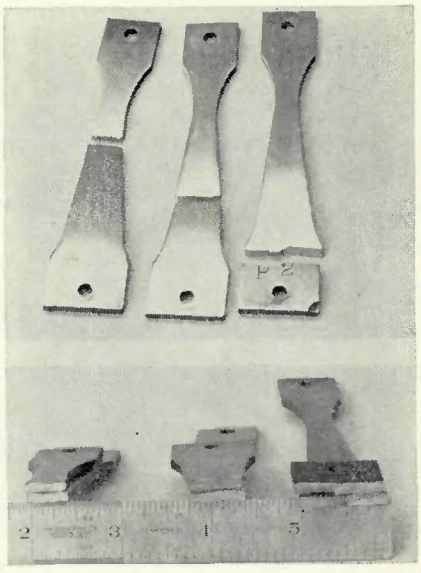

Fig. 16—Three fatigue fractures. Right—unwelded specimen with failure in vise clamp initiated by stamp; center—typical failure in unwelded tapered section; left—typical failure in welded specimen occurring in middle of specimen

was superior to the arc-furnace melted material at stresses below 105,000 psi and consequently longer fatigue lives.

Microhardness traverses proved to be an effective method of determining the metallurgical changes in the heat-affected zone. In the as-welded condition, microhardness traverses revealed extremely large changes in hardness across the heat affected zone. Hofmann *et al.*[5] suggested that this pronounced zone in itself produced a notch affect, thus initiating premature failure. Meier[1] proposed that since the zone was so narrow, it was in effect supported by the surrounding material and had little affect on the mechanical properties of the entire weldment. Figures 3–5 indicate the heat-affected zone in all three materials was exceedingly narrow, but greatly dissimilar to the unaffected base metal in hardness.

Fusion Zone and Solidification Mechanics

First, it is noted that in the as-welded and postheat-treated condition a definite dendritic structure was observed in the fusion zone (Fig. 7), although in the postheat-treated condition the weld centerline was not very definite. Dendrities seemed to be interwoven in the heat-treated condition. McHenry has attributed the premature fatigue failure in D6AC steel to this solidification pattern. Alerting the pattern did result in superior fatigue properties.[7] In the present investigation both the definite dendrite centerline pattern and subsequent fatigue failure in the center of the fusion zone were not observed. On the contrary the fatigue failure was initiated adjacent to the fusion line, although it propagated in some instances across the fusion zone (Fig. 15).

In all fatigue tests, both welded and unwelded specimens included, it was observed that a definite endurance limit did not exist within the test range examined. Fatigue ratios at 1.5×10^6 cycles (fatigue strength/ultimate tensile strength) for the three materials ranged from a maximum of 0.41 for the vacuum melted PH 14-8 Mo to a minimum of 0.34 for the arc-furnace melted PH 15-7 Mo. As a comparison the welded specimens exhibited a fatigue ratio of 0.375 for PH 14-8 Mo Vac Melt at 0.5×10^6 cycles. This ratio could not be calculated for the PH 15-7 Mo, but was less than 0.35 for the arc melted PH 14-8 Mo at 0.4×10^6 cycles. These calculations show that notch sensitivity of these materials is extremely high since only small changes in hardness could account for the variation in the fatigue performances of the welded materials.

Conclusions

1. Fatigue properties determined for PH 14-8 Mo, PH 14-8 Mo Vac Melt, and PH 15-7 Mo precipitation hardening stainless steels indicated that no definite endurance limit was reached within the maximum test range of 1.5×10^6 cycles.

2. Fatigue properties of unwelded specimens could be rated in terms of the fatigue ratio at 1.5×10^6 cycles. Maximum fatigue performance was recorded by the PH 14-8 Mo Vac Melt stainless steel with the other materials following in a decreasing order of fatigue performance.

3. A comparison between vacuum melting and arc-furnace melting processes indicated that the vacuum melting process accounted for a 20 to 30% increase in the fatigue life of PH 14-8 Mo stainless steels.

4. Fatigue joint efficiencies of 40 to 75% were recorded for the PH 14-8 Mo Vac Melt, while efficiencies of 30 to 54% were recorded for the PH 14-8 Mo specimens.

5. Fatigue joint efficiencies could not be calculated for the PH 15-7 Mo. From the scattered data it could be determined that the fatigue joint efficiencies were comparable to the PH 14-8 joint efficiencies.

6. The small hardness variations exhibited just within the limits of the fusion zone were believed to be connected with premature fatigue failure in electron beam welded specimens. It was concluded that fatigue cracks could nucleate and propagate in this softer region at lower stress levels, thus causing the premature failures.

Acknowledgement

The authors wish to thank the Armco Steel Corporation for supplying the raw material.

Bibliography

1. Meier, J. W., "High Density Electron Beam Welding," *Assembly and Fastener Engineering*, March, (1963).

2. Hashimoto, T. and Matsuda, R., "Unique Feature of Bead Shape and Its Formation Process in Electron Beam Welding," *Welding Research Abroad*, No. 8, (1965).

3. Hashimoto, T. and Matsuda, F., "Penetration Mechanism of Weld Bead in Electron Beam Welding," *Welding Research Abroad*, February, (1966).

4. Roth, R. E., Bratkovich, and Purdy, R. E., "Electron Beam Welding-Applications and Design Considerations for Aircraft Turbine Engine Gears," Welding Journal, **44** (8), 631 to 640 (1965).

5. Hofmann, W., Koch, H., and Seeler, H., "A Study of Electron Beam Welding-Process and Materials," *Welding Research Abroad*, No. 4, (1964).

6. McHenry, H. I., "Mechanical Properties of Electron Beam Welded D6AC Steel," General Dynamics/Fort Worth, *Report FGT-5250*, (1966).

7. McHenry, H. I., "Material Evaluation-Electron Beam Welded D6AC Steel Subsequently Heat Treated to the 260-280 KSI Range-Mechanical Properties," General Dynamics/Fort Worth, *Report FGT-3221*, (1966).

8. *Product Data Armco Steel*, "Armco Precipitation Hardening Stainless Steels, Sheets and Plate," (1960), "Armco Precipitation Hardening Stainless Steel PH 14-8 Mo, Sheets and Strip," (1966).